NASA TECHNICAL NOTE

NASA TN D-3602
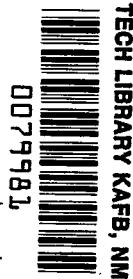
NASA TN D-3602

BLADE ELEMENT PERFORMANCE OF AXIAL-FLOW PUMP ROTOR WITH BLADE TIP DIFFUSION FACTOR OF 0.66

by Max J. Miller and Donald M. Sandercock

Lewis Research Center
Cleveland, Ohio

BLADE ELEMENT PERFORMANCE OF AXIAL-FLOW PUMP ROTOR

WITH BLADE TIP DIFFUSION FACTOR OF 0.66

By Max J. Miller and Donald M. Sandercock

Lewis Research Center
Cleveland, Ohio

NATIONAL AERONAUTICS AND SPACE ADMINISTRATION

BLADE ELEMENT PERFORMANCE OF AXIAL-FLOW PUMP ROTOR

WITH BLADE TIP DIFFUSION FACTOR OF 0.66

by Max J. Miller and Donald M. Sandercock

Lewis Research Center

SUMMARY

A 9-inch-diameter axial-flow rotor with an 0.8 hub-tip radius ratio and a design diffusion factor of 0.66 at the rotor tip was tested in water. Detailed measurements of the radial distributions of flow conditions at the rotor inlet and outlet, and performance and flow parameters across a number of selected blade elements are presented. Visual observations made during cavitating flow conditions are correlated with performance results.

The data indicate that secondary flows had a significant effect on blade-element flow and performance parameters. The unusually low values of loss in the blade hub and mean regions combined with the sharp gradients in the tip region are believed indicative of the radially outward transport of blade surface boundary layer. Variations of deviation angle can also be qualitatively explained from secondary flow effects on turning angle for a blade with a radially increasing blade section circulation.

The rotor did not quite produce design head rise, primarily because measured deviation angles were higher than those predicted by the design procedure at all radii except in the hub regions.

Where possible, measured reference values of incidence angle (e.g., minimum-loss values) for each blade element were selected and were compared with values computed from two-dimensional cascade correlations for the same flow and blade geometry. The differences represent the types of first-order correction for three-dimensional effects currently applied in the design and analysis systems.

At design flow, inlet pressure was reduced in discreet steps until the overall head rise had decreased approximately 10 percent from the noncavitating value. Radial distributions of blade-element flow and performance parameters are presented at four levels of inlet pressure.

INTRODUCTION

A reduction in the number of stages comprising a pump configuration usually means reductions in weight, matching problems, and mechanical complexity. The number of stages required to obtain a desired overall pump head rise is minimized when each individual stage is designed to produce the maximum possible head rise. Hydrodynamic limitations to the amount of head rise that can be produced by a single stage generally arise from considerations of cavitation, blade loading, stable operating range, and blade stall characteristics. The applicability and importance of each limitation to a given blade row will vary with the purpose of the individual stage in the pump and the requirements placed on the overall pump by the mission.

The Lewis Research Center has conducted a study of the effect of blade loading on the performance characteristics of axial flow stages. This study has been carried out by making detailed measurements of flow at the entrance and exit of each blade row. These measurements provide necessary information to set attainable performance levels, to provide better understanding of flow patterns over a range of operating conditions, and to furnish data for application to design and performance analysis procedures. Throughout this study, a measure of the blade loading is provided by means of a diffusion factor, or D-factor, which is developed in reference 1. Performance of typical axial-flow pump rotors with blade tip D-factors of 0.25 and 0.43 are reported in references 2 to 5. In order to extend the study, an experimental investigation of a rotor with a design blade-tip D-factor of 0.66 was conducted.

The blade-element design procedure for this 0.66-D-factor rotor is presented in reference 6, together with the measured overall performance under both noncavitating and cavitating conditions and limited measurements taken with the rotor operating in unstable flow regimes. In the present report, a more detailed analysis of the performance of the same rotor is made. Since this type of rotor normally operates in a noncavitating environment, primary attention is focused on operation under noncavitating conditions. Variations of flow conditions and performance of a selected number of blade elements over a range of operating modes are presented. Measured values are compared with design values. The measured results, which reflect three-dimensional flow effects, are also compared with values computed from prediction procedures based on correlations of two-dimensional data. The differences provide first-order correction factors for three-dimensional flow effects for application in design and analysis procedures. Performance data taken at a limited number of operating points under cavitating conditions are also presented.

APPARATUS AND PROCEDURE

Test Rotor

The design of the rotor used in this investigation is discussed in detail in reference 6, and a photograph of the rotor is shown in figure 1. The rotor tip diameter was 9 inches and was combined with a hub-tip radius ratio of 0.8 to give a blade height of 0.9 inch. The design value of ideal inlet flow coefficient (no correction for wall boundary-layer blockage) was 0.466. The design also assumed that the flow coefficient was constant radially and the inlet flow had no prewhirl (β_1 = 0).

The velocity diagrams at the rotor outlet were designed to produce nearly constant radial distributions of head rise and flow coefficients; to accomplish this, an energy addition increasing from hub to tip was applied. The blade-tip diffusion factor was 0.66. All significant design velocity diagram parameters are presented in reference 6.

Blade design followed the method advanced in reference 7. A double-circular-arc blade shape with a chord of 1.49 inches was prescribed for all radial stations. Additional blade design parameters are listed in table I. To aid in defining blade nomenclature, a schematic diagram relating flow velocity vectors to blade parameters is given in figure 2. All symbols are defined in appendix A.

C-65-2020

Figure 1. - Rotor.

TABLE I. - BLADE DESIGN VALUES

[Number of blades, 19; radial tip clearance, 0.016 in.; leading
and trailing edge radii, 0.010 in.]

Radius ratio, r/r_t	Incidence angle, i, deg	Deviation angle, δ, deg	Camber angle, φ^o, deg	Solidity, σ	Setting angle, γ, deg	Ratio of maximum thickness to chord, t_{max}/c
1.00	-3.5	7.5	27.0	1.00	55.0	0.070
.95	-4.8	11.0	35.8	1.05	50.7	.075
.90	-5.1	13.7	42.7	1.11	46.2	.080
.85	-3.4	13.8	42.6	1.18	43.3	.085
.80	-1.7	15.0	43.4	1.25	39.8	.090

Test Facility

Performance tests of this rotor were carried out in the Lewis water tunnel. A schematic diagram of the facility is shown in figure 3, and a description of the facility is given in reference 2. Before the tests, the water in the loop was conditioned by reducing the gas content to approximately 1 part per million by weight and by circulating the water through a filter capable of removing solid particles larger than 5 microns. During tests, gas content was maintained below 3 parts per million by weight, and water temperature was held constant at approximately 80° F. A schematic of the pump inlet flow path is shown in figure 4.

Test Procedure and Instrumentation

The noncavitating performance characteristic was obtained by maintaining the inlet pressure and rotative speed constant while varying flow. At each selected flow the radial distributions of flow conditions were surveyed at measuring stations located approximately 1 inch upstream of the blade leading edge and 5/8 inch downstream of the blade trailing edge. Measurements of total pressure, static pressure, and flow angle were recorded at radial locations approximately 5, 10, 20, 30, 50, 70, and 90 percent of the passage height from the outer walls (designated RP-5, 10, 20, 30, 50, 70, and 90, respectively). Blade elements were assumed to lie on cylindrical surfaces intersecting these radial positions.
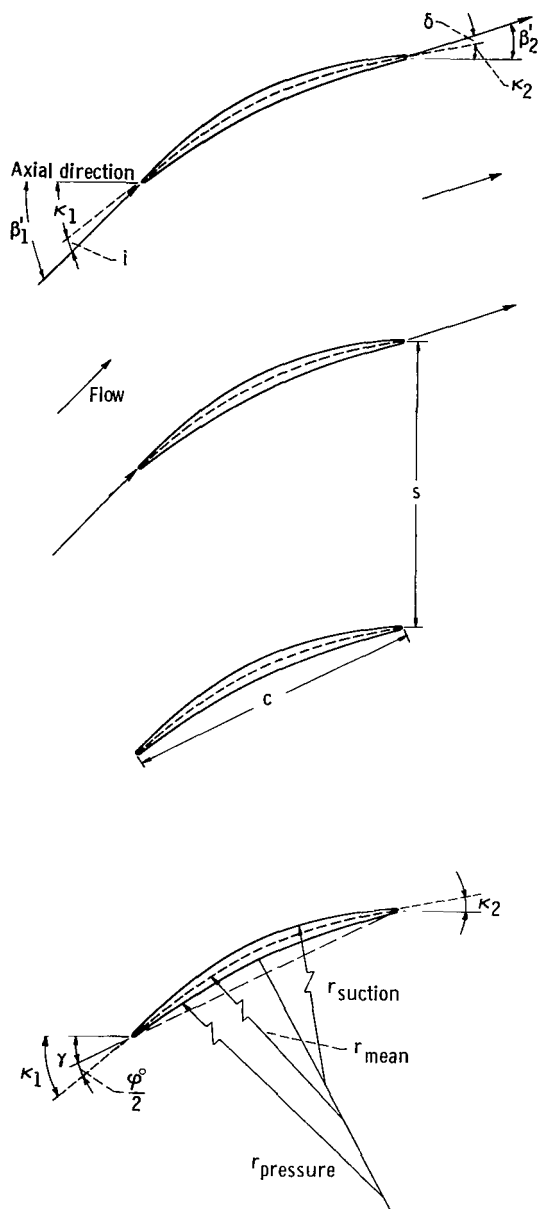
Figure 2. - Blade nomenclature.

Figure 3. - Schematic diagram of test loop.
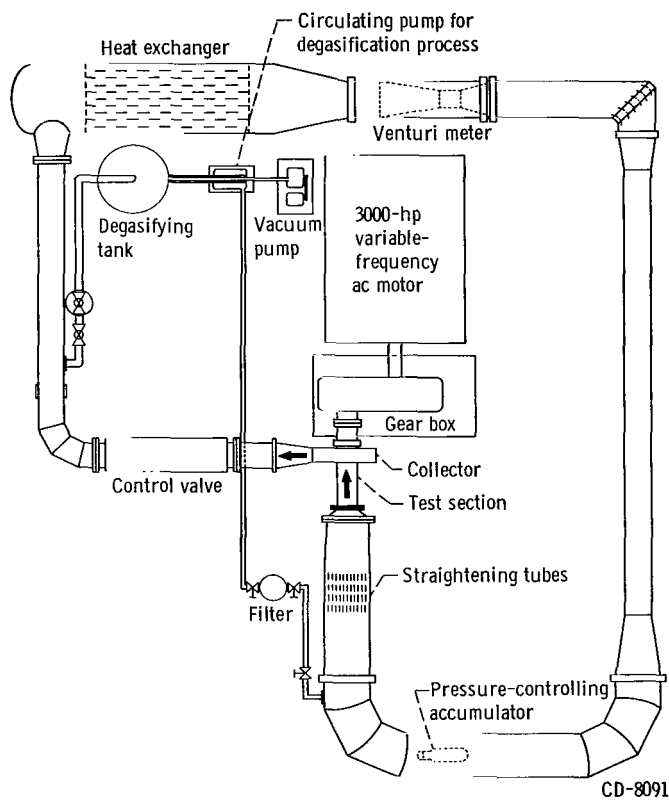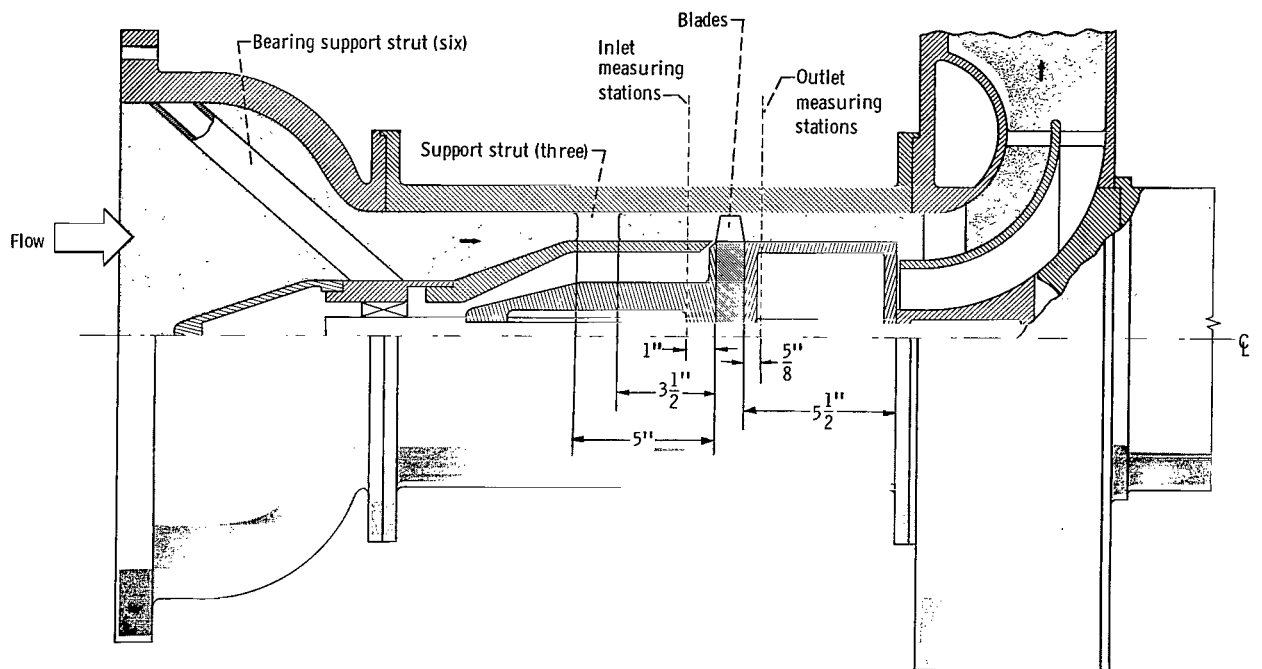
CD-8091

5

Figure 4. - Schematic diagram of inlet flow path and test section.

(a) Outlet total-pressure and flow-angle claw.

(b) Static-pressure wedge.

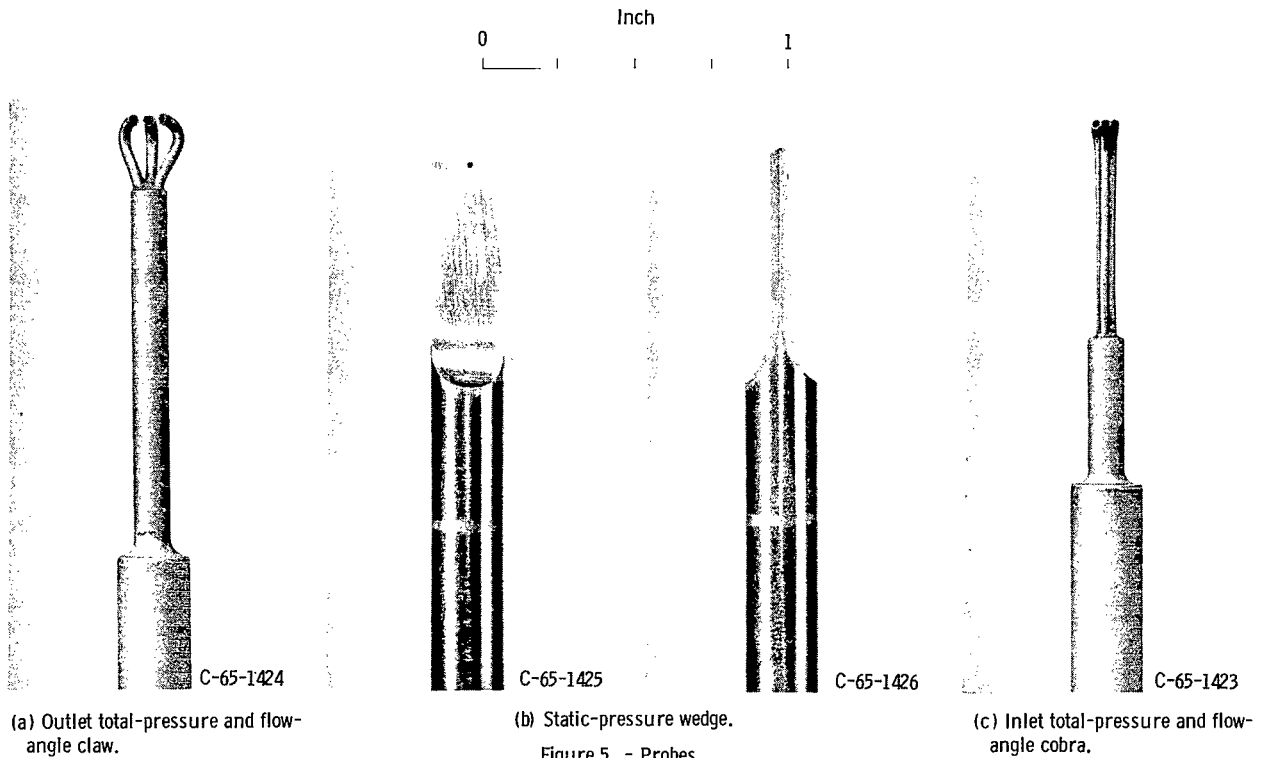(c) Inlet total-pressure and flow-angle cobra.

Figure 5. - Probes.

Cavitation performance was obtained by using the following test procedure. Blade speed and flow were held constant while inlet pressure (therefore, H_{sv}) was systematically reduced from a high (noncavitating) value. At approximately design flow, passage surveys were taken at several selected values of inlet pressure, including one at which the rotor head rise had decreased from its noncavitating value by approximately 10 percent.

Photographs of the survey probes used to measure pressures and flow angle are shown in figure 5. All probes were automatically alined with the flow direction by means of a null balance system. Static-pressure probes were calibrated in a low-speed air tunnel. System instrumentation included a Venturi meter, a water temperature recording device, a shaft speed pickup used in conjunction with an electronic counter, and an inlet pressure transducer.

The equations for calculating the selected blade element and overall performance parameters are presented in appendix B.

Data Accuracy and Reliability

The estimated accuracies of the data based on inherent accuracies of the measuring and recording devices are as follows:

Flow rate, Q_v, percent of rotor design flow . . . . ±1.0
Rotative speed, N, percent . . . . ±0.5
Blade element head rise, ΔH, percent at design flow . . . . ±1.0
Velocity head, $V^2/2g$, percent at design flow . . . . ±1.5
Flow angle, β, deg . . . . ±1.0
Net positive suction head, H_{sv}, ft . . . . ±1.0
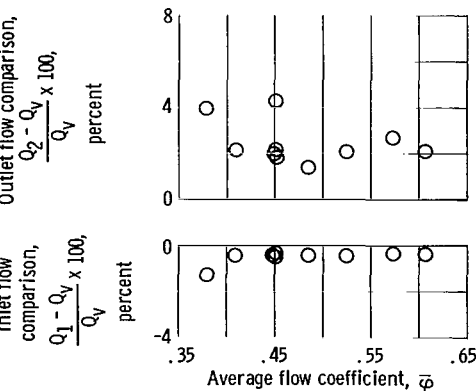

Figure 6. – Comparison of integrated flows at blade inlet and outlet with those measured by Venturi meter.

The influences of secondary flows, unsteady flows, circumferential variations of flow, etc. on the accuracies of the data could not be evaluated.

The primary method for determining the reliability of the measured data is through comparisons of the integrated weight flows at the blade inlet and outlet measuring stations with the values measured with the Venturi meter. These comparisons are presented in figure 6. With one exception, integrated flows at the inlet measuring station were within ±1 percent of the Venturi measured flows, while at the outlet measuring station

7

all integrated flows were within ±4.5 percent and the majority of them were within ±2.5 percent. Flow comparisons of this magnitude are well within the values of approximately ±3 percent at the inlet and ±5 percent at the outlet generally experienced in similar single stage tests.

Examination of the output parameters indicated that negative loss coefficients were computed for a number of blade elements and flow conditions. A review of the measurement system indicated that the probable source for computing these unrealistic flow conditions lay in the outlet flow angle. The review further indicated that the inherent accuracy value of $\pm 1^{\circ}$ noted previously was not exceeded, but that the problem lay in the ability of a single measurement of outlet flow angle to represent a true circumferential average value. For the low values of fluid flow angle at the blade outlet, a small variation in flow angle β_2 results in significant changes in V_{θ}, ψ_i, and η (sin β_2), but small changes in V_z and Q (cos β_2). For example, if β_2 is 25°, a 2° increase will change sin β_2 approximately 6 percent, while cos β_2 will be changed only approximately 2 percent. Therefore, a small discrepancy between the measured outlet flow angle and the true circumferential average angle could lead to negative loss coefficients ($\eta > 100$ percent) over low-loss portions of the blade, even though the integrated weight flow compared closely with that measured by the Venturi.

Blade Element Data

A set of experimental blade element data relates measured flow changes to a blade section of known geometry. A factor which affects the interpretation of the data is the method of relating the blade geometry to the change in flow conditions. An obvious additional factor, the data accuracy and its effect on the various blade element parameters, is discussed in the previous section. In general, measured flow changes are related to blade section geometry by assuming that (1) the flow is axisymmetric, and (2) the flow stream surfaces through the blade row lie along the same conical or cylindrical surfaces (of known blade geometry) at all operating conditions. It is recognized that three-dimensional effects (radial flows, gradients of flow conditions, secondary flows, blade tip clearance flows, etc.) will cause deviations between the actual streamline flows and the idealized stream surfaces based on these assumptions.

The effects of these measurement problems are evidenced by the band of data that results when large amounts of both two-dimensional and three-dimensional results are correlated. First-order three-dimensional correction factors can be utilized to reduce the scatter. From the remaining narrower bands of data, specific trends and average values of parameters can be deduced.

The concepts of the preceding discussion were considered in the interpretation of the

particular set of data presented herein. Correlation of this set of data with data from similar rotors would be expected to yield a narrow band of data. Thus, the trends from this set of data can be used to identify certain flow phenomena and to explain blade-row performance variations. The quantitative value of the individual blade-element parameter, however, represents only one value of the narrow band and should be used with caution.

In this investigation, slightly negative loss coefficients across certain blade elements have been calculated. A specific reason for this obviously unrealistic condition could not be established, although a probable cause is advanced. However, the trends are considered valid, and since the interpretation of the blade-element performance data follows the reasoning just given, the negative values calculated across a few blade elements do not seriously detract from the worth of the data presented or from the applicability and utility of the blade element concept.

RESULTS AND DISCUSSION

The results are presented in three parts: (1) annulus boundary layer measurements, (2) noncavitating performance, and (3) cavitating performance. In general, the plots presented are self-explanatory, and only significant features are discussed.

Annulus Boundary Layer Measurements

As a part of the investigation, outer casing boundary layers at the blade inlet and outlet measuring stations were approximated from total head surveys of the boundary layer made with the normal survey instrumentation and from a wall static-pressure measurement. The effects of the head gradient on the measurements were accounted for by the method presented in reference 8. Some typical results are shown in figure 7. At RP-10 the velocity gradient at both the inlet and the outlet is that associated with the free stream rather than the boundary layer. Blade element performance computed at this station is not considered to be unduly influenced by casing boundary layer flow. The inlet profile indicates some slight decrease from the free stream total head at RP-5. At this radial station, inlet casing boundary layer flow does exercise some influence on blade element performances. The difference in boundary layer velocity profiles at the inlet and outlet probably reflects the action of the rotor blade to energize the flow in the tip region.

In order to determine the measured $\bar{\varphi}$ required to produce the design inlet velocity diagrams, the inlet casing boundary layer blockage was estimated. The concept of displacement thickness was applied to the outer casing velocity profile and to an inner
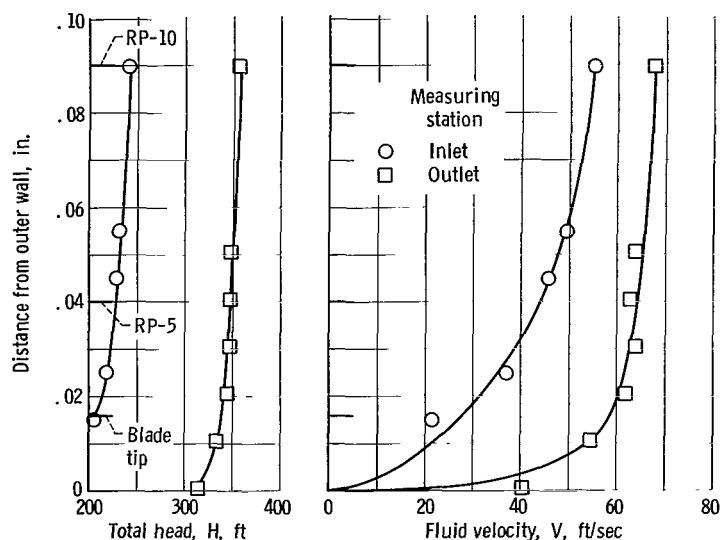
Figure 7. - Typical outer wall boundary-layer velocity and total head profiles as measured with normal survey instrumentation. Flow coefficient, 0.451.
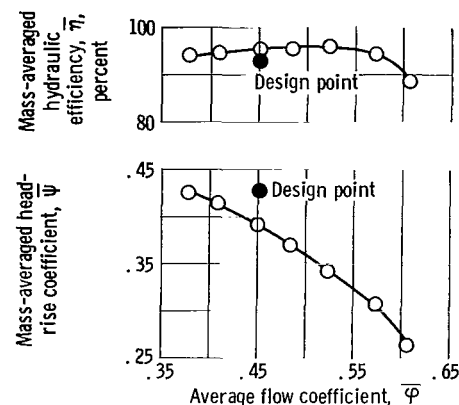
Figure 8. - Overall performance of axial-flow-pump rotor for non-cavitating conditions. Rotor tip speed, 118 feet per second.

casing velocity profile which was assumed to be similar. A blockage factor of approximately 3 percent of the annulus area was calculated. Since the annular wall boundary layers reduce the effective flow area, the design inlet velocity diagrams were met at a $\bar{\varphi}$ lower than the design φ_i. For comparison with design, performance and flow conditions at a measured overall flow coefficient of $\bar{\varphi} = 0.97\varphi_i = 0.97(0.466) = 0.452$ were used.

Noncavitating Performance

The procedure for determining a noncavitating inlet pressure is discussed in reference 6. Applicable net positive suction head values are given with each data plot.

Overall performance. - The overall performance is presented in figure 8, in which mass-averaged values of head rise coefficient and hydraulic efficiency are plotted as functions of average inlet flow coefficient. All parameters are defined in appendix B. The results presented are discussed in reference 6; consequently, only a brief resume is given herein for correlation with the more detailed blade element performance. The following summarizes the results presented in reference 6 and indicated in figure 8:

(1) At the design flow coefficient of 0.452, the measured head rise coefficient $\bar{\psi}$ of 0.391 was 8.4 percent below the design value of 0.427. However, the measured efficiency (95.5 percent) was approximately 3 percent higher than the predicted design value (92.8 percent).

(2) A high value of efficiency was maintained over a large portion of the flow range covered.

10

(3) Blade stall flow coefficient ($\overline{\varphi}$ = 0.379) was approximately 84 percent of the design flow coefficient ($\overline{\varphi}$ = 0.452). Additional stall data presented in reference 6 indicated that 0.379 represents an accurate blade stall flow coefficient.

Radial distributions. - The radial distributions of selected flow and performance parameters at four flow coefficients are presented in figure 9. Plots such as these permit a detailed examination of blade performance. The discussion in this section is directed to general performance trends indicated by the data and applicable to all operating
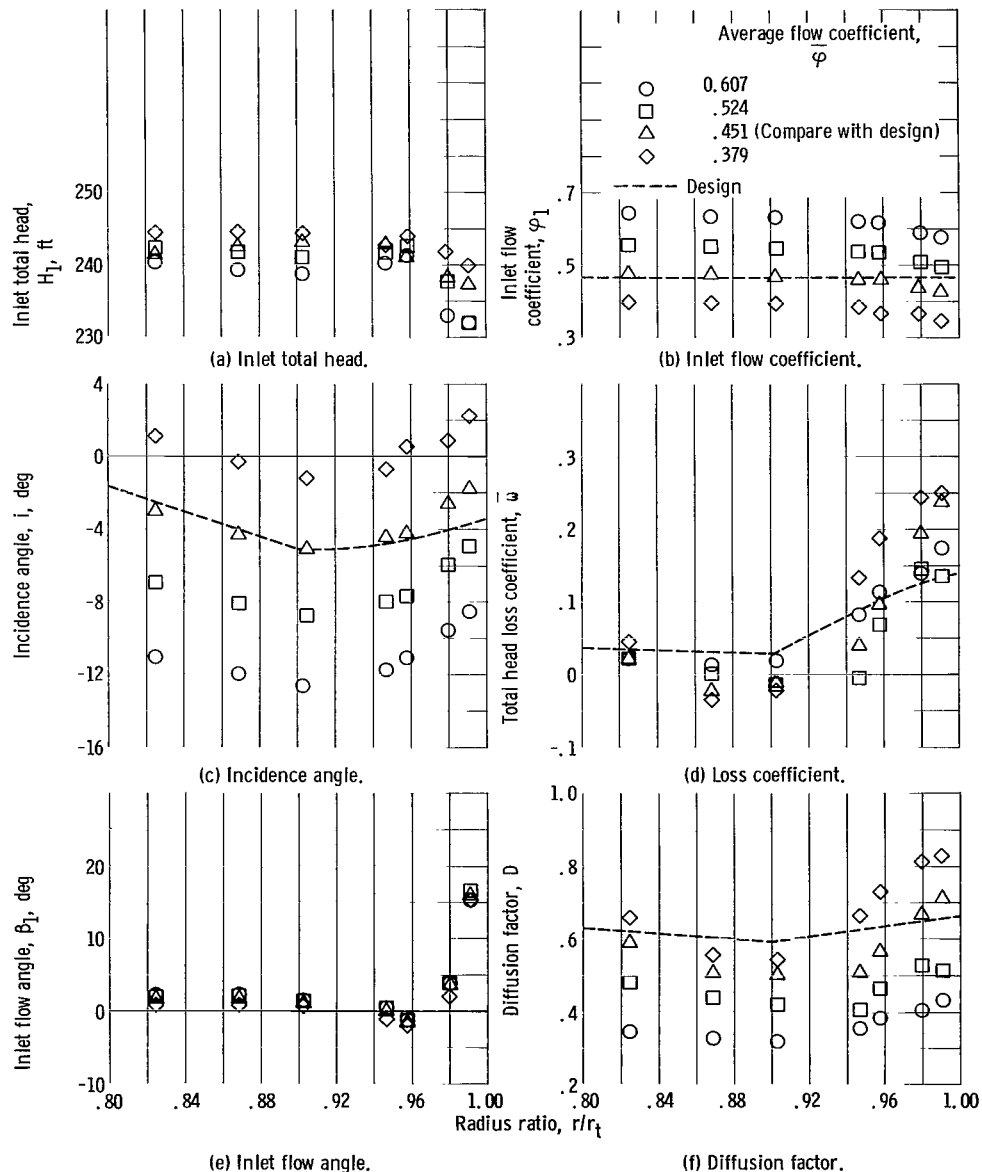

Figure 9. - Radial distributions of blade-element flow and performance parameters (noncavitating). Rotor tip speed, 118 feet per second; net positive suction head, 239 feet.

(g) Hydraulic efficiency.

(h) Ideal head-rise coefficient.

(i) Outlet flow angle.

(j) Deviation angle.

(k) Head-rise coefficient.

(l) Outlet flow coefficient.
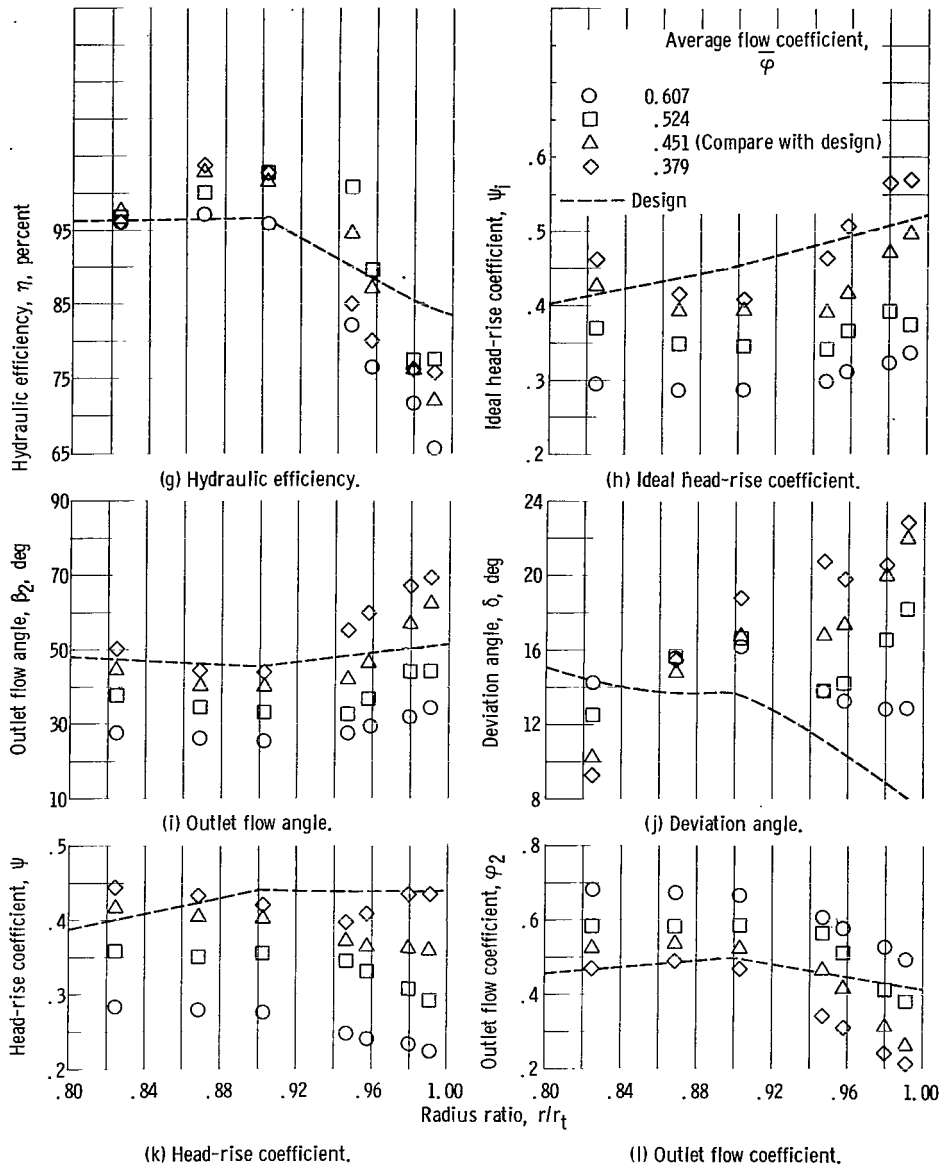
Figure 9. – Concluded.

points. A specific comparison of measured and design performance is made in the section Comparison with design.

At the blade inlet, the total head (fig. 9(a)) drops off in the tip region because of outer wall boundary layer effects; this cause for the drop is confirmed by the boundary layer survey results discussed previously. This decrease in total pressure results in a decrease in flow coefficient (fig. 9(b)) and tends to increase incidence angle (fig. 9(c)). The latter trend is counteracted to some extent by the positive whirl (positive inlet flow angle) measured in the tip region, which tends to decrease incidence angle.

The radial distributions of loss coefficient (fig. 9(d)) show a consistent pattern at all

12

flows. Low levels of loss were measured in the hub and mean regions with very sharp increases in the blade tip regions. Sources of this high loss in blade tip region include (1) profile loss associated with high D-factors, (2) blade tip clearance flow losses, and (3) secondary flow losses. It was not possible to determine the contribution of each of these sources to the measured overall loss level. However, the combination of high loss in the tip region and very low loss in the mean and hub regions is interpreted as evidence of secondary flow, particularly radial outward transport of blade surface boundary layer.

The most striking feature of the radial distributions of deviation angles (fig. 9(j)) is the general tendency to increase with radius. In contrast, prediction of the deviation angles for the individual blade elements on the basis of two-dimensional cascade correlations (ref. 7) would result in a radial distribution decreasing from hub to tip, similar in trend to the design distribution. One source for increasing deviation angles as measured in the blade tip region is the high level of blade loading (D-factor) with its associated higher level of loss, which may be indicative of thickened blade suction-surface boundary layer and possible local separation. The highest values of loss coefficient (fig. 9(d)) and deviation angles do occur at the same flow coefficient ($\bar{\varphi} = 0.379$). This flow is very close to the stalling flow, and the blade elements operate at conditions where local flow separations are likely to occur. At higher flows, as the blade elements approach the minimum-loss operating condition, the deviation angles do not decrease consistently as loss decreases at a given radial position.

Deviation angles may also be affected by the secondary flows in the blade passages, which induce changes in the direction of the through flow or main stream flow. An airfoil theory approach to these induced flow effects is based on the trailing vorticity associated with the spanwise variations of circulation. A qualitative discussion of secondary flows and their induced effects is given in reference 9. As might be expected, the secondary flows will be strongest in the hub and tip regions, where casing boundary layer, blade tip clearance flows, etc. all tend to complicate the flow patterns. The discussion herein is primarily concerned with the radial distributions in flow regions outside of those strongly affected by casing boundary layer and blade tip clearance flows, that is, in the so-called potential flow region where blade element data apply. In this region, blade spanwise distribution of circulation is represented by the radial variations of ideal head rise coefficient ψ_i (fig. 9(h)). It is shown in reference 9 that, generally, for circulation increasing with radius, an underturning (increased δ) will occur in the tip region and an overturning (decreased δ) will occur in the hub region as compared to the fluid turning angle predicted from two-dimensional considerations. The opposite trends accompany an inverse radial distribution of circulation. At present, the results reported in reference 9 are applied only qualitatively. No attempt is made to obtain the two-dimension fluid turning (deviation angle) that each blade element would produce under similar inlet flow conditions. In general, the radial distributions of ideal head rise coefficient ψ_i (fig. 9(h))

indicate that, as flow is reduced, the differences between the tip and hub values of circulation increase and the gradients become steeper, particularly in the blade tip region. At the high flow, the radial distribution of circulation approaches the free vortex distribution ($rV_\theta = c$), and three-dimensional flow effects are minimized. At this high flow, the deviation angle distribution is generally similar to the variation that would be predicted from two-dimensional correlations. As flow is decreased and the circulation gradients increase, the consistent increase and decrease in deviation angle in the tip and hub regions, respectively, seem to reflect the relative underturning in the tip and over-turning in the hub predicted in reference 9 as effects of secondary flows.

Comparison with design. - For comparison with design, the measured performance at an average flow coefficient of 0.451 (fig. 9) is used. At the blade inlet, the measured and design flow conditions are reasonably close except at $r/r_t = 0.99$, where the casing boundary layer is significantly affecting the flow. Inlet flow angles (fig. 9(e)) are within $\pm 2^\circ$ of the design assumption of no prewhirl ($V_{\theta,1} = 0$) at all stations except where $r/r_t = 0.98$ and 0.99. Measured inlet flow coefficients (fig. 9(b)) meet design values at all radii except near the tip where casing boundary layer causes a slight decrease. For this reason, the tip region incidence angles (fig. 9(c)) are slightly increased over the design values.

Although the design procedure predicted an increase in loss (fig. 9(d)) from the mean to the tip, it did not anticipate either the sharp gradient or the high level of loss measured in the tip region. Except for the tip region, measured loss coefficients are generally lower than the design values.

Measured deviation angles (fig. 9(j)) were higher than design predicted values at all radii except in the hub region. These higher-than-design levels of deviation angle mean that the design turning of the fluid was not achieved and they are the primary reason this rotor did not achieve either its design energy addition or head rise, as indicated by ψ_i and ψ in figures 9(h) and (k), respectively.

The high level of losses in the tip region and the need for the flow to satisfy radial equilibrium and continuity requirements caused a sharp decrease in outlet flow coefficient (fig. 9(l)) below the design level in the tip region. This decrease in outlet flow coefficient tends to increase the energy addition (and therefore ψ_i) in the tip region; however, only at the hub element was design energy addition attained (fig. 9(h)). The combination of loss and energy addition resulted in a radial distribution of blade-element head rise decreasing slightly from hub to tip (fig. 9(k)). Only at the hub element was the design head rise realized. Because of the sharp decrease of axial velocity in the tip region, design D-factor (fig. 9(f)) was realized at the tip element ($r/r_t = 0.98$). However, an undesirable proportion of the design level of D-factor was obtained from diffusion of relative velocity ($1 - V_2'/V_1'$) of equation (B8) rather than from change in V_θ ($\Delta V_\theta / 2\sigma V_1'$ of eq. (B8)), which would have further increased the energy addition. Loading at all other

14
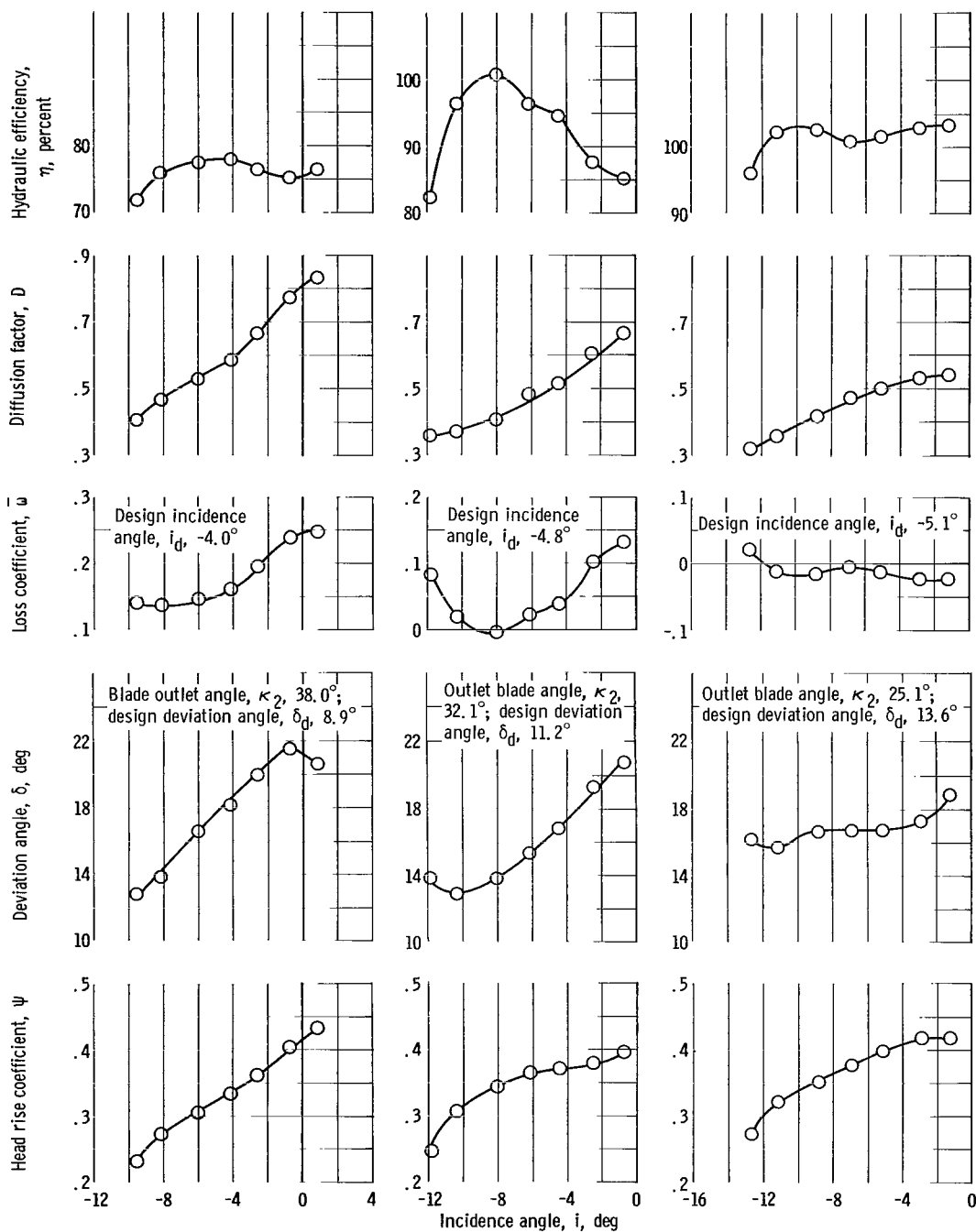
(a) Blade element located at 10 per-
cent of passage height from tip.
Radius ratio, 0.980.

(b) Blade element located at
30 percent of passage
height from tip. Radius
ratio, 0.947.

(c) Blade element located 50 percent
of passage height from tip. Radius
ratio, 0.903.

Figure 10. – Rotor blade-element performance characteristics (noncavitating). Rotor tip speed, 118 feet per second;
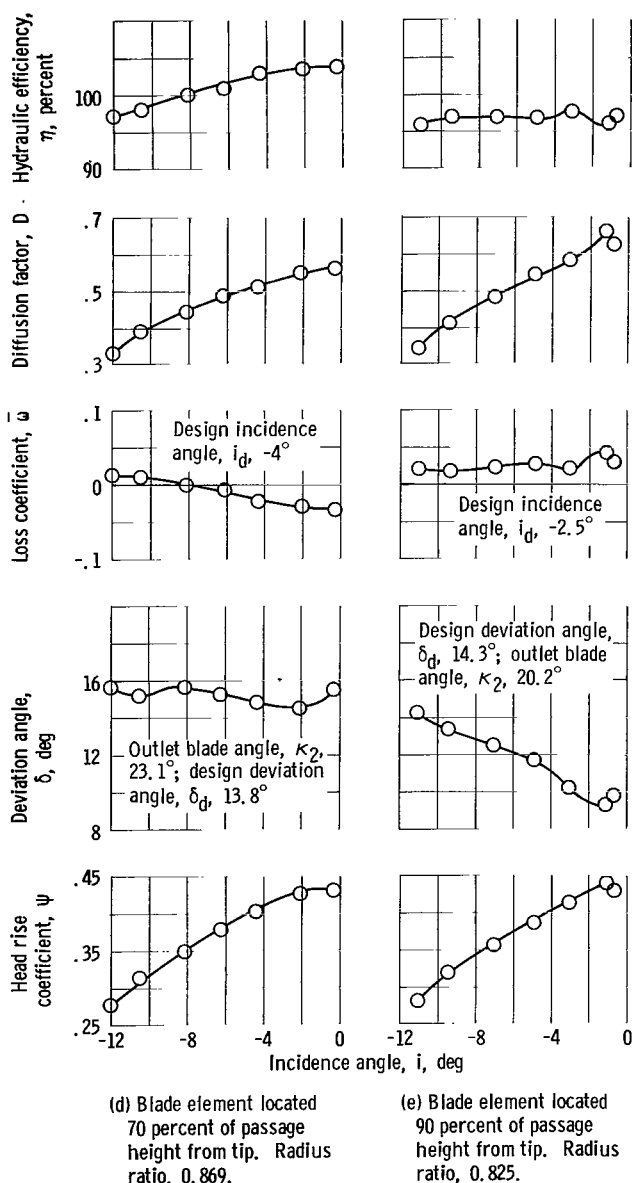net positive suction head, 239 feet.

15

Hydraulic efficiency, η, percent

100

90

Diffusion factor, D

.7

.5

.3

Loss coefficient, $\bar{\omega}$

.1

Design incidence angle, i_d, -4°

0

-.1

Design incidence angle, i_d, -2.5°

Deviation angle, δ, deg

16

Outlet blade angle, κ_2, 23.1°; design deviation angle, δ_d, 13.8°

12

8

Design deviation angle, δ_d, 14.3°; outlet blade angle, κ_2, 20.2°

Head rise coefficient, ψ

.45

.35

.25

-12   -8   -4   0

-12   -8   -4   0

Incidence angle, i, deg

(d) Blade element located 70 percent of passage height from tip. Radius ratio, 0.869.

(e) Blade element located 90 percent of passage height from tip. Radius ratio, 0.825.

Figure 10. - Concluded.

blade elements fell below the design values.

Blade element performance. - The variations of selected blade-element performance parameters with incidence angle are presented in figure 10 for five blade elements designated as RP-10, 30, 50, 70, and 90. Blade-element characteristic curves such as these provide the basic information for channeling into design and analysis programs. Primary interest is in loss coefficient $\bar{\omega}$, deviation angle δ, and incidence angle i. Where applicable, design values of the parameters are included.

For design point application, element performance at some reference incidence angle is of interest. One widely used reference incidence angle is the minimum-loss incidence angle. For the data presented herein, minimum-loss incidence angles were defined at the two blade elements representing the upper 30 percent of the blade span (RP-10 and 30), but over the remainder of the blade span, low loss was obtained over almost the entire flow range covered by this investigation, and minimum-loss incidence angles could not be designated. The performance characteristics at both RP-10 and 30 indicate that the minimum-loss incidence angle was slightly less than the design value, or, based on these two blade elements, that minimum loss should occur at a slightly higher flow than design. Blade element efficiency is related to both the blade section loss $\bar{\omega}$ and the energy input ψ_i in the form

$$\eta = 1 - \frac{\text{loss}}{\text{energy input}}$$

Thus, the maximum efficiency occurs when the ratio of loss to energy input is a minimum

value and is not necessarily coincident with the minimum-loss operating point. The blade-element efficiency variations generally reflect this relation and the blade overall efficiency results from a summation of the blade element values. As noted previously, the measured values of deviation angle were higher than the design values at all elements except the hub element.

For application to off-design prediction methods, the variation of deviation angle with incidence angle (flow) is of interest. At the tip element (RP-10) the deviation angle increases very sharply with incidence angle (fig. 10). In fact, the deviation angle is increasing at approximately the same rate as the incidence angle; thus, the blade element fluid turning $\Delta\beta'$ remains approximately constant as incidence angle increases (becomes less negative). However, the element circulation ΔV_θ will increase with incidence angle because of the decrease in axial velocity as flow is reduced (incidence angle increases). Thus, the energy addition (ψ_i in fig. 9) and the blade loading, as indicated by D-factor, continue to increase.

The variation of deviation angle with incidence angle at the hub element (RP-90, fig. 10) is in sharp contrast to that observed at the tip element. As incidence angle is increased (flow decreased) the measured deviation angle decreases significantly. Between the hub and tip elements the variations of deviation angle with incidence angle show a consistent trend between the two extremes. The trends of deviation angle with incidence angle evidenced by this rotor are believed to be primarily influenced by secondary flow effects, as discussed previously, at least over the incidence angle range where losses have not become excessive ($\overline{\omega} \geq 2\,\overline{\omega}_{m\ell}$). In particular, the trends noted are associated with a blade row which has increasing circulation from hub to tip. The three-dimensional effects on reference incidence and deviation angles must be accounted for in design procedures. One method is to modify two-dimensional deviation and reference incidence angles with three-dimensional correction factors based on data from similar rotors (ref. 7). For example,

$$i_{ref} = i_{2\text{-D}} + (i_{ref} - i_{2\text{-D}})$$

and

$$\delta_{ref} = \delta_{2\text{-D}} + (\delta_{ref} - \delta_{2\text{-D}})$$

where $i_{2\text{-D}}$ and $\delta_{2\text{-D}}$ are computed from correlation of two-dimensional cascade data (ref. 7), and $(i_{ref} - i_{2\text{-D}})$ and $(\delta_{ref} - \delta_{2\text{-D}})$ are empirical three-dimensional correction factors. The three-dimensional correction factors are obtained from single-stage test results.

In general, the reference angles (i_{ref} and δ_{ref}) are the minimum-loss values

measured for each blade element. From the data obtained in this investigation, minimum-loss incidence angles for blade elements in the outer portion of the blade span (RP-10 and 30) were reasonably well defined and were used as the reference incidence angle. At the other blade element locations, an initial attempt to obtain a reference incidence angle was to select a low-loss range of incidence angles and to designate the midrange value as the reference incidence angle. However, it was recognized that, in all instances, this low-loss range was a portion of the flow range covered in this investigation, and may not represent a complete low-loss range as bounded by well defined negative and positive stall incidence angles. For these blade elements, the high and low values of incidence angle that define the selected low-loss range, as well as the midrange value, are all presented. Selected values of reference incidence and reference deviation angles (i_{ref} and δ_{ref}), together with the related blade section two-dimensional values as computed by the methods of reference 7, are summarized in table II. Computed values of three-dimensional corrections ($i_{ref} - i_{2-D}$) and ($\delta_{ref} - \delta_{2-D}$), as well as loss coefficient $\bar{\omega}$, diffusion factor D, and a loss parameter $\bar{\omega} \cos \beta_2' / 2\sigma$ (ref. 7), are included when they are meaningful.

The data in table II indicate that the three-dimensional minimum-loss incidence angles (i_{ref}) in the blade tip region are slightly more negative than the two-dimensional values (i_{2-D}); thus, they require a negative three-dimensional correction factor. In the mean and hub region blade elements, more than one reference incidence angle was selected from the low loss incidence angle range. For each reference incidence angle selected, a corresponding three-dimensional correction factor was computed and presented to show the dependence of the correction factors on the reference incidence angle value selected.

The calculated three-dimensional correction factors for application to design deviation-angle prediction procedures indicate generally that positive values should be applied in the tip region and the magnitude should be reduced continuously as the radial location of the blade element decreases. At the hub location, the three-dimensional and two-dimensional values of deviation angle are essentially the same. The data from this rotor indicate that the spanwise gradient of circulation should be considered when determining the magnitude and radial variation of correction factors in any design.

Across the tip element, the measured values of loss coefficient $\bar{\omega}$, and loss parameter $\bar{\omega} \cos \beta_2' / 2\sigma$ fall within the range of values measured for axial flow compressors and reported in references 1 and 7, respectively. In general, at the other radii, the values presented herein are lower than those measured at similar stations of compressor blading.

Adjusted performance data. - It is noted previously that small deviations of the measured fluid flow angles at the blade outlet from a circumferential average value could significantly affect the quantitative levels of a number of blade element parameters. In this

18

Radial position of blade element, RP, percent of passage height from outer wall	Radius ratio, r/r_t	Measured reference incidence angle, i_{ref}, deg	Two-dimensional reference incidence angle, i_{2-D}, deg	Three-dimensional correction factor, $(i_{ref} - i_{2-D})$, deg	Measured reference deviation angle, δ_{ref}, deg	Two-dimensional reference deviation angle, δ_{2-D}, deg	Three-dimensional correction factor, $(\delta_{ref} - \delta_{2-D})$, deg	Total-pressure loss coefficient at measured reference incidence angle, $\overline{\omega}_{ref}$	Total-pressure loss parameter at measured reference incidence angle, $\left(\dfrac{\overline{\omega}\cos\beta_2'}{2\sigma}\right)_{ref}$	Diffusion factor at measured reference incidence angle, D_{ref}
10	0.980	-8.0	-4.7	-3.3	14.0	10.7	3.3	0.135	0.041	0.465
30	0.947	-8.0	-5.5	-2.5	13.8	12.6	1.2	-----	-----	-----
50	0.903	-1.2	-8.5	7.3	18.8	15.2	3.6	-----	-----	-----
	.903	-5.6	-7.1	1.5	16.6	13.9	2.7	-----	-----	-----
	.903	-10.0	-6.0	-4.0	16.0	12.8	3.2	-----	-----	-----
70	0.869	-0.3	-7.6	7.3	15.4	14.8	0.6	-----	-----	-----
	.869	-5.0	-6.2	1.2	15.0	13.4	1.6	-----	-----	-----
	.869	-10.0	-5.0	-5.0	15.2	12.3	2.9	-----	-----	-----
90	0.825	-3.0	-5.3	2.3	10.2	13.1	-3.0	-----	-----	-----
	.825	-7.0	-4.4	-2.6	12.5	12.2	.3	0.020	0.007	0.482
	.825	-11.0	-3.6	-7.4	14.3	11.4	2.9	-----	-----	-----

section, adjustments are applied to the fluid outlet flow angles and an adjusted set of blade element parameters is calculated. Comparison of the adjusted and as-measured values illustrates the magnitude of the effect of small variations of outlet flow angle on various blade-element parameters.

A consistent adjustment applied directly to angle measurements was not indicated from a review of the data, instrumentation, test procedures, etc. Consequently, new velocity diagrams, which applied an adjustment indirectly to β_2, were computed for each blade element by means of the following procedure:

(1) Adjusted axial velocities were computed by multiplying the measured axial velocities by the ratio of the Venturi-measured to integrated flows, or

$$V_{z, 2, a} = \left(\frac{Q_v}{Q_2}\right) V_{z, 2}$$

(2) Adjusted outlet flow angles were computed by assuming that the measured absolute velocities were correct, or

$$\beta_{2, a} = \cos^{-1} \frac{V_{z, 2, a}}{V_2}$$

(3) Complete velocity diagrams were computed from the adjusted values of flow angle $\beta_{2, a}$, measured values of velocity V_2, and measured values of blade speed U_2.

Adjusted values of blade-element performance parameters were calculated from measured inlet flow conditions, measured head rise, and the adjusted outlet velocity diagrams. Mass-averaged values of adjusted ideal head-rise coefficient $\overline{\psi}_{i, a}$ were also calculated to show effect on mass-averaged efficiency. The as-measured and adjusted values of selected blade-element performance parameters are compared by means of the radial distributions presented in figure 11. The magnitude of the change in outlet flow angle is also indicated in figure 11. Comparisons of the blade element parameters indicate the following:

(1) In all cases the trend of the parameter with radius is maintained.

(2) Largest changes in parameter values occur at the highest flow coefficient.

(3) Use of the adjusted velocity diagrams results in loss coefficients which have positive values, but, in general, the values remain low.

(4) Deviation angles were changed a maximum of approximately 1^O with most changes of $1/2^O$ or lower.

These comments also apply to comparisons of the blade element characteristic curves obtained by plotting the parameters against the incidence angle.
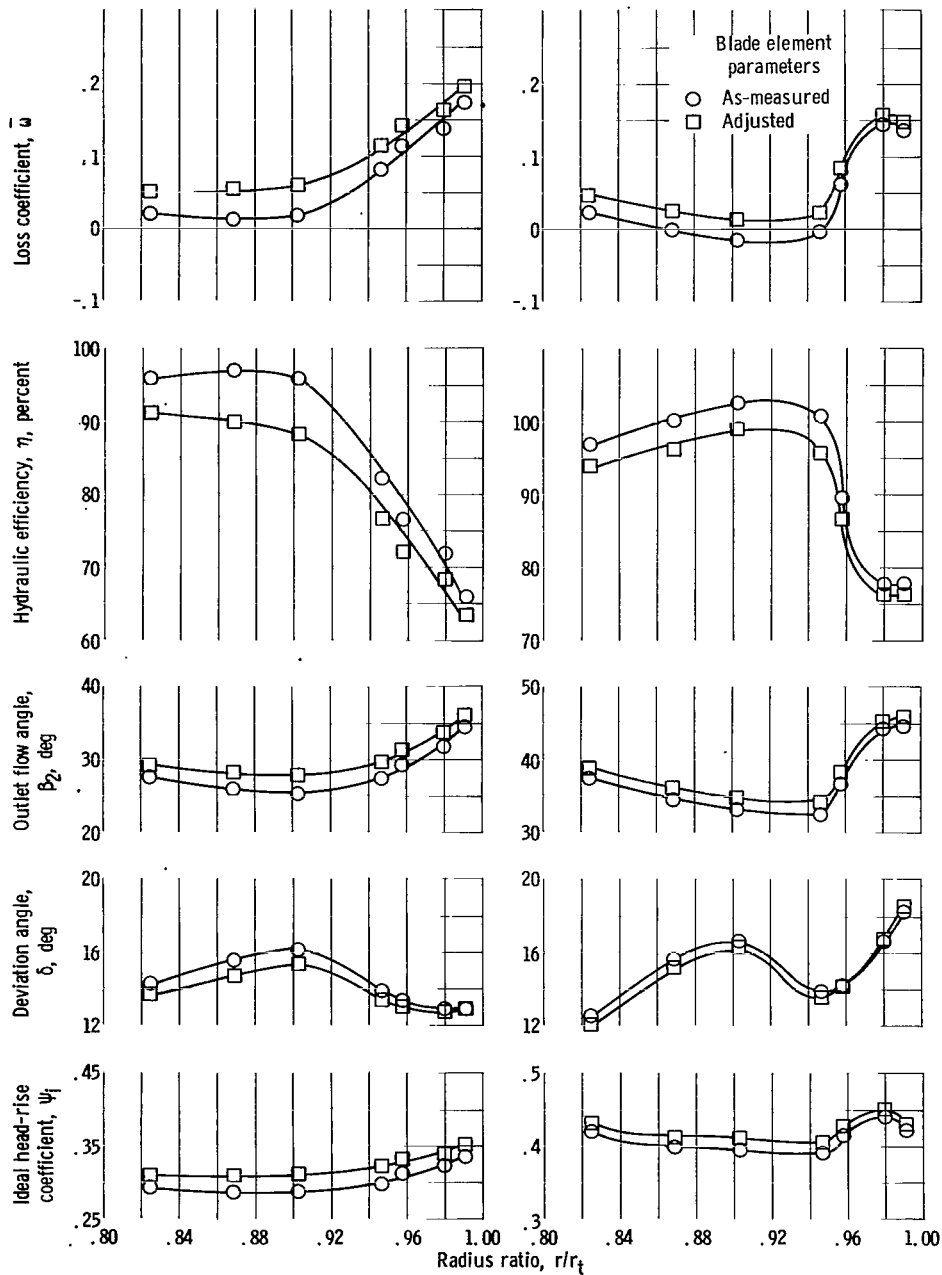
20

(a) Average flow coefficient, 0.607.　　　　(b) Average flow coefficient, 0.524.

Figure 11. – Comparison of as-measured and adjusted blade element parameters.

(c) Average flow coefficient, 0.451.
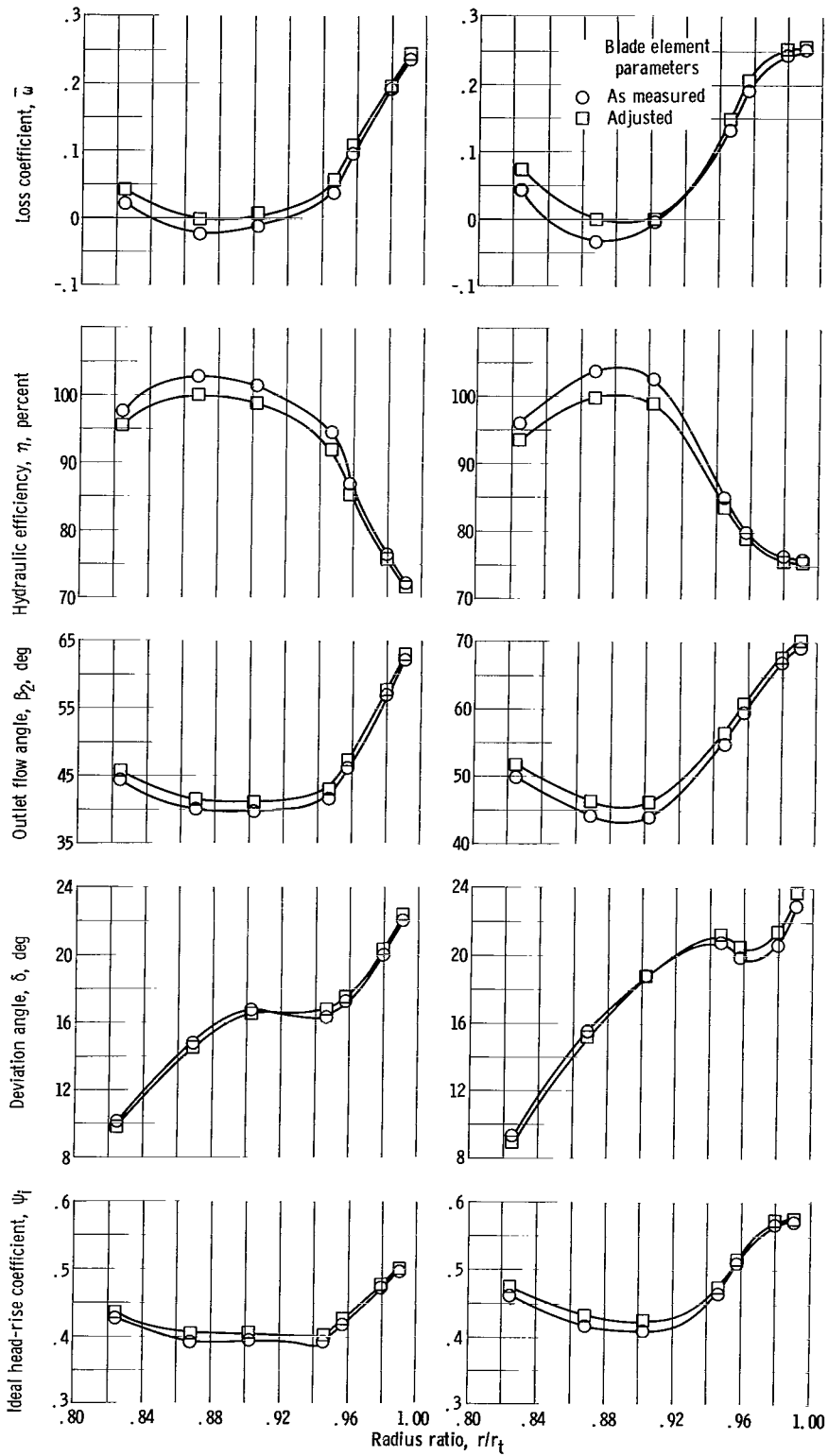
(d) Average flow coefficient, 0.380.
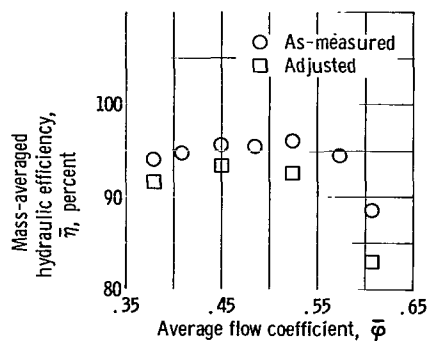
Figure 11. – Concluded.

Figure 12. - Comparison of overall
efficiencies computed from as-
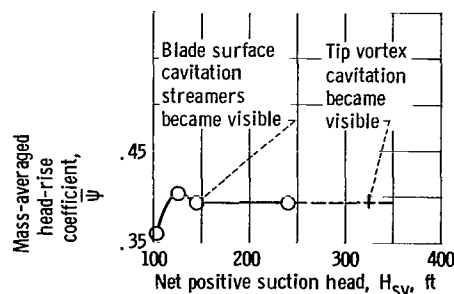measured and adjusted data.

Figure 13. - Axial-flow-pump per-
formance as function of net
positive suction head. Rotor tip
speed, 118 feet per second;
average flow coefficient, 0.451.

The effect of applying the adjustments on the mass-averaged value of efficiency is shown in figure 12, in which the adjusted and as-measured values are compared. The adjusted values indicate that the maximum efficiency would drop from 95.5 to 93.4 percent and occur closer to the design flow as compared with the as-measured results.

Cavitating Performance

Cavitating performance of this type of rotor is of interest primarily to establish the level of inlet pressure needed in order that the rotor may operate free of cavitation at design flow. Mass-averaged performance at design flow over a range of reduced inlet pressures and the 10 percent blade element performance over a range of inlet pressures and flows are presented in reference 6. The overall mass-averaged performance is repeated herein in figure 13. In addition, the radial distributions of selected blade-element performance parameters at design flow and at decreasing levels of inlet pressure are presented in figure 14.

The discussion of both measured performance and visual observations made during the investigation will follow the sequence of decreasing levels of inlet pressures (therefore H_{sv}) used to study cavitation effects on this rotor. At all H_{sv} values presented, flow conditions at the inlet to the rotor were maintained constant, as indicated by the lack of measurable change in the radial distributions of incidence angle (fig. 14(b)). The performance and flow parameters will be discussed primarily as to their deviations from the noncavitating values which have been plotted in figure 14 for comparison. At this flow coefficient ($\overline{\varphi} = 0.451$), noncavitating flow conditions are assumed to occur at all H_{sv} values greater than 146 feet for $U_t = 118$ feet per second.

At $H_{sv} = 146$ feet, the initial formation of blade surface cavitation was observed in the blade midspan regions. The cavities appeared as streamers initiated at approximately the midchord location. Loss coefficients (fig. 14(a)) rose slightly and deviation
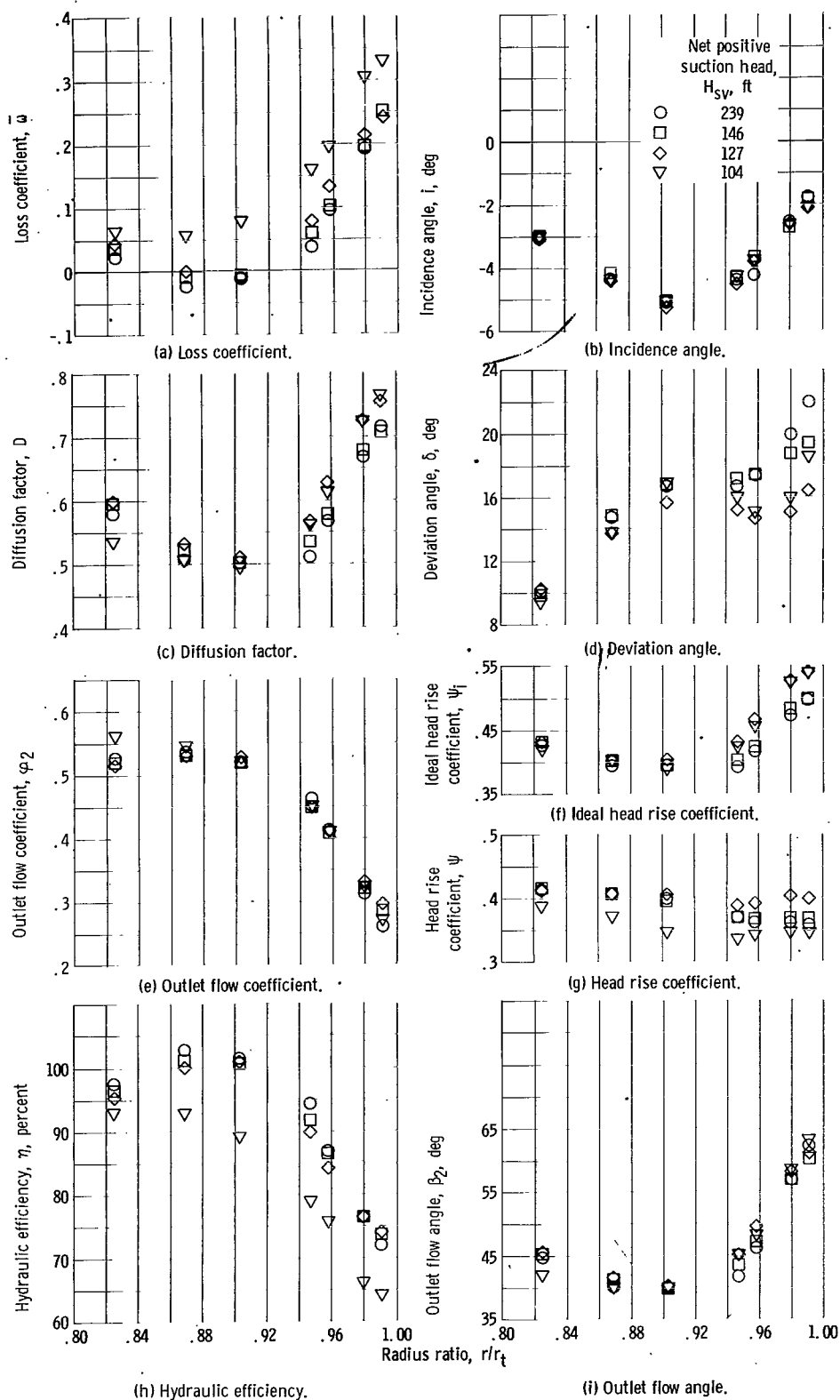
23

Figure 14. - Radial distributions of flow and blade element parameters as net positive suction head is reduced. Rotor tip speed, 118 feet per second; average flow coefficient, 0.451.

24

angles decreased slightly in the tip regions. The level of mass-averaged performance was not affected.

At $H_{sv} \approx 127$ feet ($\bar{k} \approx 0.32$), blade surface cavitation spread into the blade hub region, but very little spread into the blade tip region. The loss coefficient (fig. 14(a)) generally increased slightly at all radii. Deviation angles (fig. 14(d)) were lower than the noncavitating values at all radii except the hub element; the most significant decreases occurred in the blade tip region. This decrease resulted in increases in level of energy addition (fig. 14(f)) and head rise (fig. 14(g)) in the tip region. The decrease in deviation angle and accompanying increase in blade element head rise explains the increase in mass-averaged head rise over the noncavitating value (fig. 13) for $H_{sv} \approx 127$ feet.

At $H_{sv} \approx 104$ feet ($\bar{k} \approx 0.23$), the cavitation spread into the blade tip region and moved forward to enclose the blade leading edge. The loss coefficient level (fig. 14(a)) increased significantly at all blade elements, with the exception of the hub region. In the blade tip region, deviation angles (fig. 14(d)) increased from the minimum values at $H_{sv} = 127$ feet but were still below the noncavitating level. In the blade mean and hub regions, deviation angles were approximately the same as the noncavitating values. Radial distribution of energy addition (fig. 14(f)) showed effects which paralleled the deviation angle effects. The head rise coefficient (fig. 14(g)) decreased from the noncavitating values at all radii. The variation of ψ and η (figs. 14(g) and (h)) at each individual blade element reflected the relative changes, or cavitation effects, on loss and energy addition.

SUMMARY OF RESULTS

A 9-inch-diameter axial flow rotor with an 0.8 hub-tip radius ratio and a blade tip design diffusion factor of 0.66 was tested in water under both noncavitating and cavitating flow conditions. As a part of the investigation, approximate definitions of the outer casing boundary layer at the blade inlet and outlet measuring stations were made. These measurements were utilized to establish a 3 percent gross flow blockage at the blade inlet. The same blockage factor was applied to the ideal design flow to determine the measured flow to be used for comparison with design. The measurements also indicated that the blade element performance computed at 10 percent of the annulus height from the outer wall was not unduly influenced by the casing wall boundary-layer flow. Blade element performance calculated from measurements taken closer to the outer wall would probably be influenced.

Detailed radial surveys of the flow conditions at the blade inlet and outlet were made, and flow and performance parameters were calculated across a number of selected blade

elements. The principal results of analysis of the blade element performance data were as follows:

1. At design flow, the rotor produced an overall head rise coefficient of 0.391 as compared with the design value of 0.427. The rotor did not meet design head rise primarily because the design underestimated deviation angle requirements at all radii except in the hub region.

2. Three-dimensional flow effects were relatively strong in this type of rotor. Loss coefficients increased very rapidly with radius in the blade tip region. This increase, combined with the unusually low loss levels in the blade mean and hub regions, was interpreted as an indication of significant secondary flows, particularly the radial outward transport of blade surface boundary layer. Measured deviation angles were considerably higher than those predicted by essentially two-dimensional empirical prediction procedures. Also, the gradients of deviation angle with incidence angle in the hub and tip regions were unusually sharp. Differences between the measured three-dimensional deviation angles and the predicted two-dimensional trends were explained qualitatively by considerations of induced flow effects of a blade row with a positive radial gradient of blade circulation.

3. In the blade mean and hub regions, the blade sections operated over a wide low-loss flow range. In the tip region, the low-loss operating range was more restricted. Measured blade parameters were compared with values computed from prediction procedures based on correlations of two-dimensional data, and the differences were presented as first-order three-dimensional correction factors for incorporation into design and analysis systems.

4. At design flow, the inlet pressure was reduced from the noncavitating value in discreet steps until a dropoff in mass-averaged head rise of approximately 10 percent was reached. The noncavitating magnitude of head rise was maintained down to a net positive suction head of 146 feet (rotor tip speed, 118 ft/sec). A further reduction of the net positive suction head to a value of 127 feet resulted in a slight increase in overall head rise primarily because of a decrease in deviation angles in the blade tip region, which increased the energy addition. At a net positive suction head of 104 feet, the overall head rise had decreased approximately 10 percent below the noncavitating level. This dropoff in overall head rise resulted from a sharp increase in loss level at all radii, which in turn caused a decrease in head rise across all blade sections.

Lewis Research Center,
    National Aeronautics and Space Administration,
        Cleveland, Ohio, May 23, 1966,
            126-15-03-28-22.

APPENDIX A

SYMBOLS

A annulus area, ft^2

c blade chord, in. (fig. 2)

D diffusion factor (eq. (B8))

g acceleration due to gravity, 32.2 ft/sec^2

H total head, ft

H_{sv} net positive suction head, ft (eq. (B18))

ΔH head rise, ft (eq. (B1))

$\overline{\Delta H}$ mass-averaged head rise, ft (eq. (B11))

h_v vapor head, ft

i incidence angle, deg (fig. 2)

$\overline{k}$ average cavitation number (eq. (B17))

N rotative speed, rpm

Q flow rate, gal/min

Q_v Venturi-measured flow rate, gal/min

RP radial position of blade element, approximate percent of passage height from outer wall

r radius, in.

s blade spacing, in. (fig. 2)

t blade thickness, in.

U rotor tangential velocity, ft/sec

V fluid velocity, ft/sec

$\overline{V}$ average fluid velocity, ft/sec (eq. (B15))

β flow angle, angle between direction of flow and axial direction, deg

γ blade setting angle, angle between chord line and axial direction, deg (fig. 2)

δ deviation angle, deg (fig. 2)

η hydraulic efficiency, percent (eq. (B5))

$\overline{\eta}$ mass-averaged hydraulic efficiency, percent (eq. (B14))

κ blade angle, angle between tangent to blade mean camber line and axial direction, deg (fig. 2)

σ blade solidity, c/s

φ flow coefficient (eq. (B6))

$\overline{\varphi}$ average flow coefficient (eq. (B16))

φ^o blade camber angle, $\kappa_1 - \kappa_2$, deg (fig. 2)

ψ head rise coefficient (eq. (B2))

$\overline{\psi}$ mass-averaged head rise coefficient (eq. (B12))

$\overline{\omega}$ rotor relative total head loss coefficient (eq. (B7))

Subscripts:

a adjusted value

d design

i $^{\backslash}$	ideal	1	rotor inlet measuring station
mℓ	minimum loss	2	rotor outlet measuring station
max	maximum	2-D	parameter obtained from correlation of two-dimensional air cascade data
ref	reference value		
t	tip		
z	axial direction		
θ	tangential direction		

Superscript:

'	relative to rotor

APPENDIX B

BLADE ELEMENT AND PARAMETER EQUATIONS

Blade Element Equations

Blade element head rise:

$$\Delta H = H_2 - H_1 \tag{B1}$$

Head rise coefficient:

$$\psi = \frac{g \, \Delta H}{U_t^2} \tag{B2}$$

Ideal head rise:

$$\Delta H_i = \frac{U_2 V_{\theta,2} - U_1 V_{\theta,1}}{g} = \frac{U_2}{g}\left[U_2 - V_{z,2} \tan(\kappa_2 + \delta)\right] - \frac{U_1 V_{\theta,1}}{g} \tag{B3}$$

Ideal head rise coefficient:

$$\psi_i = \frac{g \, \Delta H_i}{U_t^2} \tag{B4}$$

Hydraulic efficiency:

$$\eta = \frac{\Delta H}{\Delta H_i} \times 100 \tag{B5}$$

Flow coefficient:

$$\varphi = \frac{V_z}{U_t} \tag{B6}$$

Rotor relative total head loss coefficient:

$$\bar{\omega} = \frac{H'_{2,i} - H'_2}{\dfrac{V'^2_1}{2g}} = \frac{\Delta H_i - \Delta H}{\dfrac{V'^2_1}{2g}}$$

(B7)

Blade diffusion factor:

$$D = 1 - \frac{V'_2}{V'_1} + \frac{r_2 V_{\theta,2} - r_1 V_{\theta,1}}{\sigma V'_1 (r_1 + r_2)}$$

(B8)

or, for $r_1 = r_2$

$$D = 1 - \frac{V'_2}{V'_1} + \frac{\Delta V_\theta}{2\sigma V'_1}$$

Incidence angle:

$$i = \beta'_1 - \kappa_1$$

(B9)

Deviation angle:

$$\delta = \beta'_2 - \kappa_2$$

(B10)

Overall and Averaged Parameter Equations

Mass-averaged head rise:

$$\overline{\Delta H} = \frac{\displaystyle\sum_{j=1}^{j=6} (r_j V_{z,2,j} \Delta H_j + r_{j+1} V_{z,2,j+1} \Delta H_{j+1})(r_j - r_{j+1})}{\displaystyle\sum_{j=1}^{j=6} (r_j V_{z,2,j} + r_{j+1} V_{z,2,j+1})(r_j - r_{j+1})}$$

(B11)

30

Mass-averaged head rise coefficient:

$$\overline{\psi} = \frac{g\,\overline{\overline{\Delta H}}}{U_t^2}$$ (B12)

Mass-averaged ideal head rise:

$$\overline{\overline{\Delta H}}_i = \frac{1}{g}\left(\overline{U_2 V}_{\theta,2} - \overline{U_1 V}_{\theta,1}\right)$$

$$= \frac{1}{g}\left(\frac{\displaystyle\sum_{j=1}^{j=6} U_{2,j} V_{\theta,2,j} A_{2,j} V_{z,2,j}}{\displaystyle\sum_{j=1}^{j=6} A_{2,j} V_{z,2,j}} - \frac{\displaystyle\sum_{j=1}^{j=6} U_{1,j} V_{\theta,1,j} A_{1,j} V_{z,1,j}}{\displaystyle\sum_{j=1}^{j=6} A_{1,j} V_{z,1,j}}\right)$$

In this investigation $V_{\theta,1}$ was considered zero in all calculations and the equation becomes

$$\overline{\overline{\Delta H}}_i = \frac{1}{g}\left(\frac{\displaystyle\sum_{j=1}^{j=6} U_{2,j} V_{\theta,2,j} A_{2,j} V_{z,2,j}}{\displaystyle\sum_{j=1}^{j=6} A_{2,j} V_{z,2,j}}\right) = \frac{\overline{U_2 V}_{\theta,2}}{g}$$ (B13)

Mass-averaged efficiency:

$$\overline{\eta} = \frac{\overline{\overline{\Delta H}}}{\overline{\overline{\Delta H}}_i} \times 100$$ (B14)

Average inlet axial velocity:

$$\overline{V}_{z,1} = \frac{144 Q_v}{448.8\pi\left(r_{t,1}^2 - r_{h,1}^2\right)}$$ (B15)

31

Average inlet flow coefficient:

$$\overline{\varphi} = \frac{\overline{V}_{z,1}}{U_t} \tag{B16}$$

Average blade cavitation number:

$$\overline{k} = \frac{2gH_{sv}}{U_t^2 \left(1 + \overline{\varphi}^2\right)} - \frac{\overline{\varphi}^2}{1 + \overline{\varphi}^2} \tag{B17}$$

Net positive suction head:

$$H_{sv} = H_1 - h_v \tag{B18}$$

REFERENCES

1. Lieblein, Seymour; Schwenk, Francis C.; and Broderick, Robert L.: Diffusion Factor for Estimating Losses and Limiting Blade Loadings in Axial-Flow-Compressor Blade Elements. NACA RM E53D01, 1953.

2. Crouse, James E.; Montgomery, John C.; and Soltis, Richard F.: Investigation of the Performance of an Axial-Flow-Pump Stage Designed by the Blade-Element Theory - Design and Overall Performance. NASA TN D-591, 1961.

3. Crouse, James E.; Soltis, Richard F.; and Montgomery, John C.: Investigation of the Performance of an Axial-Flow-Pump Stage Designed by the Blade-Element Theory - Blade-Element Data. NASA TN D-1109, 1961.

4. Crouse, James E.; and Sandercock, Donald M.: Design and Overall Performance of an Axial-Flow-Pump Rotor with a Blade Tip Diffusion Factor of 0.43. NASA TN D-2295, 1964.

5. Crouse, James E.; and Sandercock, Donald M.: Blade-Element Performance of 0.7 Hub-Tip Radius Ratio Axial-Flow-Pump Rotor with Tip Diffusion Factor of 0.43. NASA TN D-2481, 1964.

6. Miller, Max J.; and Crouse, James E.: Design and Overall Performance of an Axial-Flow Pump Rotor with a Blade-Tip Diffusion Factor of 0.66. NASA TN D-3024, 1965.

7. Johnsen, Irving A.; and Bullock, Robert O., eds.: Aerodynamic Design of Axial-Flow Compressors. NASA SP-36, 1965.

8. Gettelman, Clarence C.; and Krause, Lloyd N.: Considerations Entering Into the Selection of Probes for Pressure Measurement in Jet Engines. Instrument Society of America, Proceedings, vol. 7, 1952, paper 52-12-1.

9. Lieblein, Seymour; and Ackley, Richard H.: Secondary Flows in Annular Cascades and Effects on Flow in Inlet Guide Vanes. NACA RM E51G27, 1951.

"The aeronautical and space activities of the United States shall be conducted so as to contribute . . . to the expansion of human knowledge of phenomena in the atmosphere and space. The Administration shall provide for the widest practicable and appropriate dissemination of information concerning its activities and the results thereof."

—NATIONAL AERONAUTICS AND SPACE ACT OF 1958

NASA SCIENTIFIC AND TECHNICAL PUBLICATIONS

TECHNICAL REPORTS: Scientific and technical information considered important, complete, and a lasting contribution to existing knowledge.

TECHNICAL NOTES: Information less broad in scope but nevertheless of importance as a contribution to existing knowledge.

TECHNICAL MEMORANDUMS: Information receiving limited distribution because of preliminary data, security classification, or other reasons.

CONTRACTOR REPORTS: Technical information generated in connection with a NASA contract or grant and released under NASA auspices.

TECHNICAL TRANSLATIONS: Information published in a foreign language considered to merit NASA distribution in English.

TECHNICAL REPRINTS: Information derived from NASA activities and initially published in the form of journal articles.

SPECIAL PUBLICATIONS: Information derived from or of value to NASA activities but not necessarily reporting the results of individual NASA-programmed scientific efforts. Publications include conference proceedings, monographs, data compilations, handbooks, sourcebooks, and special bibliographies.

Details on the availability of these publications may be obtained from:

SCIENTIFIC AND TECHNICAL INFORMATION DIVISION

NATIONAL AERONAUTICS AND SPACE ADMINISTRATION

Washington, D.C. 20546